Complex field-induced states in Linarite $PbCuSO_4(OH)_2$ with a variety of high-order exotic SDW_p states

B. Willenberg[1,2], M. Schäpers[3], A.U.B. Wolter[3], S.-L. Drechsler[3], M. Reehuis[2], B. Büchner[3,4], A.J. Studer[5], K.C. Rule[5], B. Ouladdiaf[6], S. Süllow[1], and S. Nishimoto[3,4]

[1] *Institute for Condensed Matter Physics, TU Braunschweig, D-38106 Braunschweig, Germany*

[2] *Helmholtz Center Berlin for Materials and Energy, D-14109 Berlin, Germany*

[3] *Leibniz Institute for Solid State and Materials Research IFW Dresden, D-01171 Dresden, Germany*

[4] *Institut für Festkörperphysik, TU Dresden, D-01062 Dresden, Germany*

[5] *The Bragg Institute, ANSTO, Kirrawee DC NSW 2234, Australia*

[6] *Institute Laue-Langevin, F-38042 Grenoble Cedex, France*

(Dated: August 15, 2016)

Low-temperature neutron diffraction and NMR studies of field-induced phases in linarite are presented for magnetic fields $H \parallel b$ axis. A two-step spin-flop transition is observed as well as a transition transforming a helical magnetic ground state into an unusual magnetic phase with sine-wave modulated moments $\parallel H$. An effective $\tilde{J}_1$-$\tilde{J}_2$ single-chain model with a magnetization-dependent frustration ratio $\alpha_{\rm eff} = -\tilde{J}_2/\tilde{J}_1$ is proposed. The latter is governed by skew interchain couplings and shifted to the vicinity of the ferromagnetic critical point. It explains qualitatively the observation of a rich variety of exotic (for strongly correlated cuprate spin-1/2 Heisenberg systems) longitudinal collinear spin-density wave SDW_p states ($9 \geq p \geq 2$).

PACS numbers: 75.10.Jm, 75.25.-j, 75.30Kz, 75.40Cx

Recently, frustrated spin chains with ferromagnetic nearest neighbor J_1 (FM-NN) and antiferromagnetic 2nd neighbor J_2 (AFM-NNN) exchange have been discussed in the context of novel states of matter. Close to the saturation field by tuning the frustration ratio $\alpha = -J_2/J_1$ of an isotropic model, a sequence of distinct spin-multipolar (MP) phases should develop with well-defined phase boundaries, which are described as a Tomonaga-Luttinger-liquid of p-magnon bound states [1–9]. They compete with exotic longitudinal spin density wave (SDW_p) correlations, which should prevail in lower magnetic fields. Interchain exchange should weaken the MP correlations, while magnetic anisotropy should stabilize them [6–9].

A proof of existence for spin-MP ordering in real quasi-1D materials is still lacking. The FM-AFM chain J_1-J_2 compound $LiCuVO_4$ was considered as a candidate, undergoing a transition into an incommensurate (ICM) helical phase below 2.1 K, into a spin-flop phase in fields of $\sim$2.5 T and an exotic SDW_2 phase above $\sim$8 T [10–13]. A shift of the SDW_2 propagation vector, consistent with longitudinal density waves of bound $p = 2$-magnons, was reported for low fields of 8–14.5 T, together with a transition from long- to short-range magnetic order [13]. It was interpreted as a signature of coexisting SDW_2 and bond-nematic order, a view disputed in Refs. [9, 14] and instead related to a pinned SDW_2. Via magnetization and NMR it was concluded that MP correlations in $LiCuVO_4$ can exist only in a narrow high field range $\sim$ 40 T [5, 15, 16].

The issue not resolved in this dispute is the relationship between SDW and MP in the long-range ordered phases appearing in 2D and 3D (in 1D the precursor "phases" overlap [3]). Theoretically, the possibility of homogeneously coexisting SDW_2 and nematic phase and/or phase separation has been suggested for the isotropic model in an extreme quasi-1D regime for specific intrachain and very weak 2D FM interchain couplings based on perturbative scattering theory [17]. In contrast, only a 1st-order phase transition was predicted for the same model [9, 14]. Also predicted is a phase separation and/or a 1st-order phase transition between nematic and FM phase in a 3D *bcc* structure for the same J_1-J_2 model and a similar approach [18] as in Ref. [17]. The situation is far from clear in $LiCuVO_4$. The phase diagram has not been studied in detail due to the high fields required to access it [19]. Further, the influence of defects on the magnetic properties is not well understood [16, 20, 21]. Thus, what is lacking in this context is a comprehensive study of a clean frustrated FM-AFM spin chain material to properly define these issues.

A unique example of a frustrated spin chain system for such studies is linarite. It crystallizes in the monoclinic space group $P2_1/m$ [22], forming buckled CuO_2 chains along the b axis. These have been modelled as a $s = \frac{1}{2}$ spin-chain with FM-NN $J_1 = -100$ K and AFM-NNN $J_2 = 36$ K [23]. In this J-parameter range the saturation field is about 10 T, allowing full experimental access to the magnetic phase diagram. For a magnetic field $H \parallel b$ axis the magnetic phase diagram contains five different regions I (elliptical helix) to V [24–26] (see Supplement). Region V displays very weak thermodynamic signatures, and it was unclear, whether it is a distinct thermodynamic phase.

Here, we fully characterize its field-induced phases by means of neutron diffraction (ND) and ^{1}H nuclear magnetic resonance (NMR). We establish the magnetic or-

dering vectors, and that region V represents a thermodynamic phase. For phase V, we determine the field dependence of the ICM SDW ordering vector and newly discover complex states which might be understood in terms of phase separation between MP and SDW_p states.

ND was carried out using the single crystal instrument D10 at the Institute Laue Langevin, France, and the instrument Wombat at ANSTO, Australia. For the D10 experiment, the sample from a previous study was used [24]. A second single crystal of linarite ($9 \times 3 \times 0.5\,\mathrm{mm}^3$) from the Grand Reef Mine, Arizona, was used for the experiment on Wombat. The samples were placed in cryomagnets with maximum field/base temperature of 6 T/1.7 K (D10) and 12 T/1.5 K (Wombat), with the magnetic field applied along the crystallographic b axis. With this setup and a neutron wavelength of 2.36 Å we were restricted along the b direction to $-0.25 < k < 0.25$ in reciprocal space for the D10 experiment, while for the experiment on Wombat a wavelength of 4.61 Å was used resulting in an access range $-0.19 < k < 0.19$.

^{1}H-NMR ($^1\gamma = 42.5749\,\mathrm{MHz/T}$) studies were performed for $T < 2.8\,\mathrm{K}$ using a phase-coherent Tecmag spectrometer in combination with a He-flow cryostat. Frequency scans were conducted down to 1.7 K and at external fields $H \parallel b$ between 1.5 T and 7.5 T. The same single crystal was used as for the D10 ND study. All NMR spectra were collected using a $\pi/2 - \tau - \pi$ Hahn spin-echo pulse sequence. The spectra have not been corrected by the tiny spin-spin relaxation time $T_2 \sim 10\mu$s.

By ND, scans of (0 k 0.5) with varying k were performed at 1.7 K for fields up to 6 T. For this temperature the sequence of phases I–III–IV is traversed with increasing field. Consistent with the 0 T propagation vector, the magnetic Bragg peak (0 −0.186 0.5) is observed at low fields (Fig. 1a). For increasing magnetic field, at the boundary to phase III a second commensurate (CM) magnetic Bragg peak appears at (0 0 0.5), corresponding to spins coupled parallel along the a and b axes and antiparallel along c. In the field range 2.60 to 2.95 T both peaks coexist, while for higher fields (in phase IV) only the commensurate Bragg peak remains.

The coexistence of two spin structures in phase III is also observed in NMR. Fig. 1b displays the absolute resonance change $\nu - \nu_0$ of the spectra taken in phase I, III, and IV (for details see Supplement). The six NMR lines in phase I are understood in terms of an ICM helical structure [26]. In phase IV four discrete resonance lines were observed. For linarite the only CM spin structure with four resonance lines is an AFM, propagating along the a or c direction, consistent with ND. Conversely, in phase III in total 12 resonance lines are detected; four with high intensity at small shifts $\nu - \nu_0 = -1.4$ to 0.5 MHz, eight lines for shifts larger than ±1.5 MHz. The four central lines resemble those of phase IV. The remaining eight peaks result from a modification of the helical phase I structure. Thus, a phase separation occurs into two spin structures. The two phases compete, as for increasing field the intensity of the central lines increase while the other decrease, reflecting a growth of the phase volume of the first on behalf of the second. The same behavior is seen for the field dependence of the corresponding Bragg peak intensities in ND (Fig. 1a).

To determine the magnetic structure with propagation vector $\boldsymbol{k} = (0\ 0\ 0.5)$ of phase IV, the intensity of 33 magnetic Bragg peaks (20 inequivalent) was measured at 4 T by ND. A refinement of the data ($R_F = 9.5\,\%$) using the program FullProf [27] reveals that the spins are lying in the ac plane, with an angle of $-27°$ off the a axis (roughly parallel to $[10\bar{1}]$), the same as one of the spin components of the phase I helix [24]. From the refinement an ordered moment of $0.79(1)\mu_\mathrm{B}$ per Cu atom is derived. Similar refinements at 5.5 T (20 inequivalent Bragg peaks) yield the same spin structure with a moment of $0.73(2)\mu_\mathrm{B}$ per Cu atom ($R_F = 12.5\,\%$). The decrease of the AFM moment with field, and the observation of small field-induced FM contributions on top of nuclear Bragg peaks, reflects the development of field-induced spin polarization.

For the determination of spin structures in phase III, two sets of magnetic Bragg peaks $(hkl)_M$ were collected at 2.8 T using the relation $(hkl)_M = (hkl)_N \pm \boldsymbol{k}$. For the ICM structure the propagation vector $\boldsymbol{k} = (0\ 0.186\ 0.5)$ was used, for the CM structure $\boldsymbol{k} = (0\ 0\ 0.5)$. The CM structure in phase III is refined using 15 peaks (14 inequivalent) with the phase IV spin model. The refinement of 18 inequivalent Bragg peaks of the ICM structure yields a circular helix structure ($R_F = 14.5\,\%$), where the moments of $0.64(2)\mu_\mathrm{B}$ lie roughly in the bc plane.

In the related chain systems $LiCuVO_4$ and $LiCu_2O_2$, applying magnetic field rotates the normal of the helical structure parallel to the field. Here, such a spin flop of

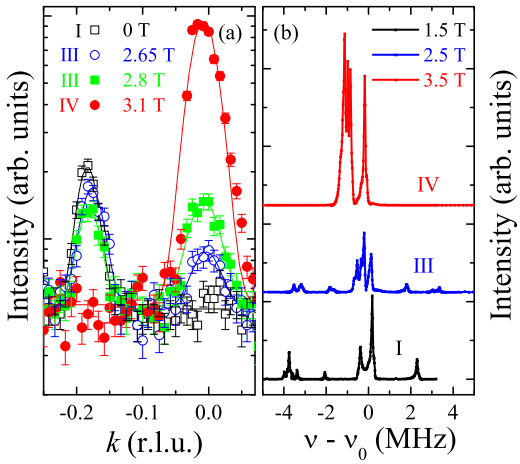

FIG. 1. a.) Neutron scattering scans for linarite along k at 1.7 K at different fields, reflecting the crossing from phase I via III into IV. Solid lines are Gaussians fitted to the data to determine peak positions. b.) NMR spectra for linarite at 1.7 K at different fields (spectra offset for clarity).

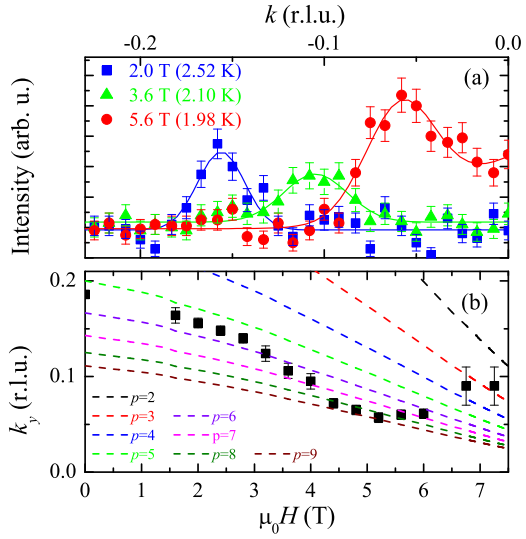

FIG. 2. a.) The magnetic Bragg peak position (0 k 0.5) shifting with field in phase V. b.) Field dependence of the propagation vector in phase V compared to the 1D model SDW$_p$ states with $2 \leq p \leq 9$. Theory lines include the magnetization obtained from $M(H,T)$ scans [25].

the helix into the ac plane is prohibited by the monoclinic angle β. Instead the spins flop into a collinear spin structure in the ac plane. In phase III the spins start to flop into the ac plane forming a collinear spin arrangement, while a coexisting helical phase is retained. The fact that in phase III a circular helix (spinning plane in the bc plane) replaces the elliptical helix reflects that for the latter it is energetically costly to keep the large moment axis aligned along the field direction. For larger fields all spins are flopped into the ac plane forming the collinear phase IV.

Next, we have performed ND via k scans through region V (Fig. 2a). Surprisingly, and in spite of the very weak signatures defining this region in thermodynamic measurements [24, 25], we observe magnetic Bragg peaks of the same width as the nuclear peaks. These peaks are even observed in the intermediate field regime $\sim 4\,$T, where in thermodynamic measurements no anomalies were detected [25]. It implies that region V is a distinct and highly unusual thermodynamic phase. For magnetic structure determination, a set of 8 inequivalent Bragg peaks was collected at 6 T. A refinement yields a sine-wave modulated structure, with the spins aligned parallel to the b axis ($R_F = 7\,\%$). Surprisingly, the SDW magnetic moment amplitude is only $0.44(1)\mu_B$. This value is much smaller than what would be expected from an extrapolation of the field dependence of the magnetic moments measured in phase I and IV. Further, the propagation vector (0 $-k$ 0.5) shifts in k with field, as shown in Fig. 2.

The sine-wave modulated structure with moments along the field direction together with the shift of the k value reminds of the prediction of the longitudinal collinear SDW within hard-core boson approximation [1, 3, 8], where the shift depends on the number of bound magnons p in the coexisting or neighboring MP phase:

$$\frac{k_y d}{\pi} = \frac{(1 - M/M_S)}{p}. \qquad (1)$$

Here, d denotes the distance of neighboring Cu spins along the b axis, M_S is the saturation magnetization [28, 29]. To compare Eq. 1 with the situation for linarite, the curves with various p values are included in Fig. 2b. Surprisingly, at first glance no agreement is found over a wide field range between the experimentally observed evolution of k_y and the theoretical prediction for a single chain with fixed field independent exchange interactions for any fixed value of p. However, taking into account the interchain coupling we will arrive at a magnetization dependent reduced effective value $\alpha_{\rm eff}(M/M_s)$. Then, the different p values seen experimentally can be qualitatively understood (see below and Supplement).

Static magnetic order in phase V of linarite is also observed by NMR. ^{1}H-NMR frequency scans were performed in the field range 3 – 7.5 T with an increment of

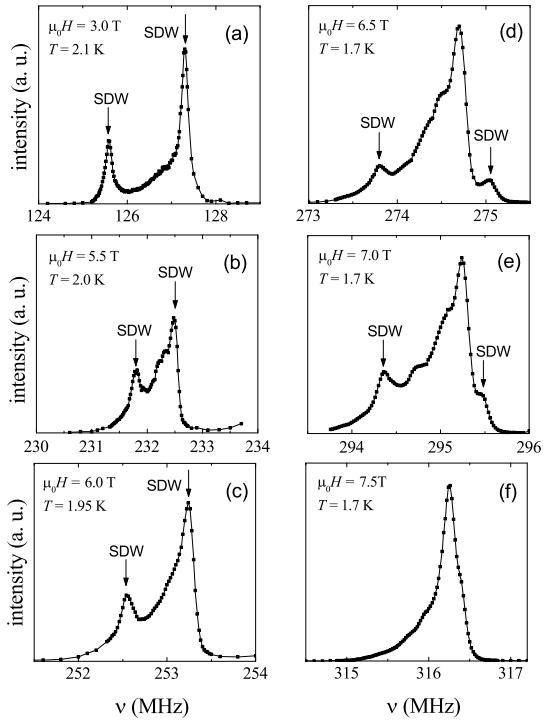

FIG. 3. The ^{1}H-NMR spectra of linarite for different magnetic fields and temperatures in phase V and in the paramagnetic polarized state at 7.5 T close to saturation.

0.5 T at different temperatures. At 2.8 K a paramagnetic signal is observed which is composed of two almost overlapping lines from two inequivalent ^{1}H sites [26]. For fields ≤ 6 T, upon lowering T below a critical value T_V the spectrum develops horn-shaped NMR characteristics, that is two distinct peaks with a finite intensity in between (Fig. 3a-c). It can be accounted for by the SDW structure with only a magnetic component along the b direction (compare $LiCuVO_4$ [16]). The transition temperatures derived from NMR match those of phase V obtained from thermodynamics for $H \parallel b$ axis [24, 25], and define the phase boundary in the field range 3.5–6 T, where no transition has been detected in thermodynamic quantities. Our findings imply that phase V encloses all other magnetic phases (see Supplement).

Increasing the field to above 6 T within phase V (in Fig. 3d/e: 1.7 K) produces a transfer of spectral weight from the horn-shaped structure to a broadened two-peak structure appearing in the middle of the SDW pattern. The shift of the latter with increasing field follows the shift of the paramagnetic polarized NMR signal close to saturation. Qualitatively, this implies the presence of two different local environments in the sample, *viz.*, a phase separation occurs. In part of the sample there is SDW ordering producing the horn-shaped NMR spectra. In contrast, the regions of the sample exhibiting the broadened two-peak structure show no static magnetic order. According to Refs. [1–3] for coupled frustrated spin chains a field-induced transition from the SDW$_p$ into a p-MP phase is expected in high fields. This transition should appear as one from a magnetically long-range ordered into one without static dipolar long-range order. Hence, we suggest that the phase separation observed in phase V is related to the transition from a SDW$_p$ phase into one with dominant MP character in a quasi-1D material.

To discuss our experimental results, we employ weakly-coupled $J_1 - J_2$ chains in a magnetic field H along the z axis. The Hamiltonian reads as

$$\hat{H} = J_1 \sum_{l,i} \mathbf{S}_{l,i} \cdot \mathbf{S}_{l,i+1} + J_2 \sum_{l,i} \mathbf{S}_{l,i} \cdot \mathbf{S}_{l,i+2} + H \sum_{l,i} S^z_i + J_{\rm ic} \sum_{l,l',i,i'} \mathbf{S}_{l,i} \cdot \mathbf{S}_{l',i'}, \quad (2)$$

where $\mathbf{S}_{l,i}$ is a spin-$\frac{1}{2}$ operator at site i in chain l and $J_{\rm ic}$ is a diagonal interchain coupling (see Fig. 4(a)). As shown above, the ICM propagation vector along the chain is $k_y = 0.186\pi$ at $H = 0$; however, a single $J_1 - J_2$ chain with $\alpha = J_2/|J_1| = 0.36$ gives $k_y \approx 0.367\pi$. This discrepancy can be resolved by taking a specific diagonal $J_{\rm ic} \approx 10\text{K} = 0.1|J_1|$. Theoretically, the propagation vector in the single J_1-J_2 chain is found from the maximum position of the static spin-structure factor $S(k)$. Due to strong quantum fluctuations and the resulting absence of static magnetic order in 1D with short range-couplings, only, it cannot be found from $< S^z_i >$. But as a precursor, the former reflects nevertheless the SDW modulations (induced by the coupling to neighboring chains in 2D and 3D) we are looking for here. This maximum position of $S(k)$ is reduced by decreasing α and it approaches 0 at the FM critical point $\alpha_c = 1/4$. Such a reduction of the propagation vector is also realized by increasing $J_{\rm ic}$ at fixed α for a system of coupled chains (see Fig. 4a and Fig. 5 in Ref. [30]). It is thus interpreted that the interchain coupling reduces the value of α. Since a single chain is more convenient than coupled chains for the discussion of MP states, we first performed a mapping from two coupled J_1-J_2 chains with $\alpha = 0.36$ and $J_{\rm ic} = 0.1|J_1|$ with periodic perpendicular boundary conditions onto an effective single $\tilde{J}_1$-$\tilde{J}_2$ chain with $\alpha_{\rm eff} = -\tilde{J}_2/\tilde{J}_1 = \alpha_{\rm eff}(\alpha, M/M_s)$. For a wide range of the magnetization $M/M_{\rm s}$ the values of $\alpha_{\rm eff}$ were estimated by fitting the dynamical spin-structure factors $S(\mathbf{q}, \omega)$. An example is shown in Fig. 4(b) (for more details see Supplement). The estimated values of $\alpha_{\rm eff}$ are plotted vs. $M/M_{\rm s}$ in Fig. 4(c). Note the vicinity to α_c.

Next, we found the number of bound magnons p for a given α by calculating the binding energy of a p-magnon bound state near the saturation field, which is defined as

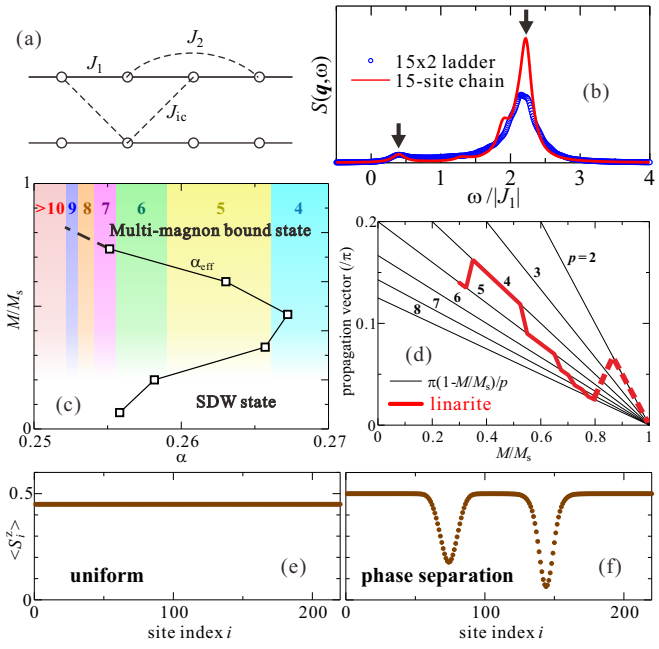

FIG. 4. (a) Lattice model of weakly-coupled $J_1 - J_2$ chains. (b) Fitting of $S(\mathbf{q}, \omega)$ at $M/M_{\rm s} = 0.2$; between $\mathbf{q} = (\pi, \pi)$ for coupled two-chain with $\alpha = 0.36$, $J_{\rm ic} = 0.1|J_1|$ and $q = \pi$ for a single chain with $\alpha_{\rm eff} = 0.257$. (c) Phase diagram of the multi-magnon bound states and the estimated effective frustration ratio $\alpha_{\rm eff}$ for linarite. (d) Suggested propagation vector using Fig. 4(c). Local spin densities $\langle S^z_i \rangle$ at $\alpha_{\rm eff} = 0.26$ and $M/M_{\rm s} = 0.95$ for (e) periodic and (f) open chains.

$$E_{\rm b}(p) = \frac{1}{p}[E(S_z = S_{\rm max} - p) - E(S_z = S_{\rm max})] - [E(S_z = S_{\rm max} - 1) - E(S_z = S_{\rm max})], \quad (3)$$

where $E(S_z = S)$ is the ground-state energy with the z component of the total spin $S_z = S$, and $S_z = S_{\rm max}$ corresponds to the fully polarized state. When the largest value of $E_{\rm b}(p)(> 0)$ is given by $p = p_{\rm max}$, we can prove that the $p_{\rm max}$-magnon bound state is the most stable state; whereas, if $E_{\rm b}(p) < 0$ for all p values no low-energy magnon bound state exists. The results are shown in Fig. 4(c). According to Refs. [1–3], the value of p increases with approaching $\alpha_{\rm eff} = 1/4$ and the region of $\alpha_{\rm eff}$ becomes narrower for larger p. Based on the relation between p and $\alpha_{\rm eff}$, the propagation vector of linarite is suggested to evolve similarly as shown in Fig. 4(d) based on calculations within our effective 1D model, in semi-quantitative agreement with the experimental data (Fig. 2(b)). For a brief discussion of the last right dashed part of the broken red lines related to $p = 2$ obtained within an analogous xyz-anisotropic Heisenberg model (to be published elsewhere) see Supplement.

The phase separation observed at high field may be attributed to the low effective frustration ratio $\alpha_{\rm eff} \approx 1/4$, i.e., close to the critical point. This means that the FM state is almost degenerate to other lower spin states. As an illustration, the local spin densities $\langle S_i^z \rangle$ with periodic and open boundaries at $M/M_{\rm s} = 0.95$ for $\alpha_{\rm eff} = 0.26$ are plotted in Figs. 4(e) and (f), respectively. A uniform distribution is naturally expected for periodic chains; whereas, interestingly, a phase separation into partial polarized and unpolarized phases occurs by open chain ends or possibly also near strong enough impurities in the bulk being a common small disorder in real materials.

To conclude, linarite exhibits a field-induced behavior generic for a FM-NN/AFM-NNN frustrated chain system. In addition, a two-step spin-flop transition is present for external magnetic fields applied along the b axis. Further, a longitudinal sine-wave modulated spin-structure phase encloses the other ordered phases. Here, at relative low fields above the helical phase a shift in the propagation vector qualitatively similar to $LiVCuO_4$ (with SDW_2 states, only) is observed. However, to the best of our knowledge we report the first observation of several exotic (for Heisenberg spin-1/2 systems) collinear longitudinal SDW_p states (by changing the external field), reaching even $p = 9$. We believe that this result is related to the appropriate bare value of α and the strong enough skew interchain coupling. Altogether, linarite appears to be a good candidate to show MP behavior. A more detailed and comprehensive study, its exotic SDW_p states, and their interplay with field-induced phase separation and exchange anisotropy provides a challenge for future work. Also the comparison with other rare cases of field-induced phase separation in frustrated zigzag chain magnetic spiral systems as $MnWO_4$ [31] is of interest for deeper insights in their complex physics including multiferroicity.

Our work has been supported by the DFG under contracts WO 1532/3-1 and SU 229/9-1. We acknowledge fruitful discussions with W. Brenig, A. Läuchli, U. Rößler, N. Shannon, O. Starykh, H. Tsunetsugu and M. Zhitomirsky. We thank G. Heide and M. Gäbelein from the Geoscientific Collection in Freiberg for providing the linarite crystal.

[1] L. Kecke, T. Momoi, and A. Furusaki, Phys. Rev. B **76**, 060407 (2007).
[2] T. Hikihara, L. Kecke, T. Momoi, and A. Furusaki, Phys. Rev. B **78**, 144404 (2008).
[3] J. Sudan, A. Lüscher, and A. M. Läuchli, Phys. Rev. B **80**, 140402 (2009).
[4] F. Heidrich-Meisner, I. McCulloch, and A. Kolezhuk, Phys. Rev. B **80**, 144417 (2009).
[5] M. E. Zhitomirsky and H. Tsunetsugu, Europhys. Lett. **92**, 37001 (2010).
[6] S. Nishimoto, S.-L. Drechsler, R. Kuzian, J. Richter, and J. van den Brink, arXiv:1005.5500 (2010).
[7] S. Nishimoto, S.-L. Drechsler, R. Kuzian, J. Richter, and J. van den Brink, arXiv:1303.1933 (2013).
[8] M. Sato, T. Hikihara, and T. Momoi, Phys. Rev. Lett. **110**, 077206 (2013).
[9] O. Starykh and L. Balents, Phys. Rev. B **89**, 104407 (2014).
[10] B. J. Gibson, R. K. Kremer, A. V. Prokofiev, W. Assmus, and G. J. McIntyre, Physica B **350**, E253 (2004).
[11] N. Büttgen, H.-A. Krug von Nidda, L. E. Svistov, L. A. Prozorova, A. Prokofiev, and W. Aßmus, Phys. Rev. B **76**, 014440 (2007).
[12] N. Büttgen, W. Kraetschmer, L. E. Svistov, L. A. Prozorova, and A. Prokofiev, Phys. Rev. B **81**, 052403 (2010).
[13] M. Mourigal, M. Enderle, B. Fåk, R. K. Kremer, J. M. Law, A. Schneidewind, A. Hiess, and A. Prokofiev, Phys. Rev. Lett. **109**, 027203 (2012).
[14] O. Starykh, Rep. Prog. Phys. **78**, 052502 (2015).
[15] L. Svistov, T. Fujita, H. Yamaguchi, S. Kimura, K. Omura, A. Prokofiev, A. Smirnov, Z. Honda, and M. Hagiwara, JETP Lett. **93**, 21 (2011).
[16] N. Büttgen, K. Nawa, T. Fujita, M. Hagiwara, P. Kuhns, A. Prokofiev, A. P. Reyes, L. E. Svistov, K. Yoshimura, and M. Takigawa, Phys. Rev. B **90**, 134401 (2014).
[17] H. Ueda and K. Totsuka, arXiv:1406.1960 (2014).
[18] H. Ueda and T. Momoi, Phys. Rev. B **87**, 144417 (2013).
[19] N. Büttgen, P. Kuhns, A. Prokofiev, A. P. Reyes, and L. E. Svistov, Phys. Rev. B **85**, 214421 (2012).
[20] L. Prozorova, S. Sosin, L. Svistov, N. Büttgen, J. Kemper, A. Reyes, S. Riggs, A. Prokofiev, and O. Petrenko, Phys. Rev. B **91**, 174410 (2015).
[21] A. Prokofiev, I. Vasilyeva, V. Ikorskii, V. Malakhov, I. Asanov, and W. Assmus, J. Solid State Chem. **177**, 3131 (2004).
[22] H. Effenberger, Miner. Petrol. **36**, 3 (1987).
[23] A. U. B. Wolter, F. Lipps, M. Schäpers, S.-L. Drechsler,

S. Nishimoto, R. Vogel, V. Kataev, B. Büchner, H. Rosner, M. Schmitt, M. Uhlarz, Y. Skourski, J. Wosnitza, S. Süllow, and K. C. Rule, Phys. Rev. B **85**, 014407 (2012).

[24] B. Willenberg, M. Schäpers, K. C. Rule, S. Süllow, M. Reehuis, H. Ryll, B. Klemke, K. Kiefer, W. Schottenhamel, B. Büchner, B. Ouladdiaf, M. Uhlarz, R. Beyer, J. Wosnitza, and A. U. B. Wolter, Phys. Rev. Lett. **108**, 117202 (2012).

[25] M. Schäpers, A. U. B. Wolter, S.-L. Drechsler, S. Nishimoto, K.-H. Müller, M. Abdel-Hafiez, W. Schottenhamel, B. Büchner, J. Richter, B. Ouladdiaf, M. Uhlarz, R. Beyer, Y. Skourski, J. Wosnitza, K. C. Rule, H. Ryll, B. Klemke, K. Kiefer, M. Reehuis, B. Willenberg, and S. Süllow, Phys. Rev. B **88**, 184410 (2013).

[26] M. Schäpers, H. Rosner, S.-L. Drechsler, S. Süllow, R. Vogel, B. Büchner, and A. U. B. Wolter, Phys. Rev. B **90**, 224417 (2014).

[27] J. Rodríguez-Carvajal, Physica B **192**, 55 (1993).

[28] Note that for linarite and $LiVCuO_4$ the lattice constant $b = 2d$ due to alternating side groups. ().

[29] The occurence of collinear SDW states with locally different collinear magnetization values is typical for intinerant magnetic systems but exotic for strongly correlated spin-1/2 systems where the magnitude of the local magnetization is fixed and the direction of the local moment changes spatially, i.e., leading either to non-collinear states or to various simple spin-up spin-down collinear Neél-states. ().

[30] S. Nishimoto, S.-L. Drechsler, R. Kuzian, J. Richter, J. Málek, M. Schmitt, J. van den Brink, and H. Rosner, EPL **98**, 37007 (2012).

[31] K. Taniguchi, M. Saito, and T. Arima, Phys. Rev. B **81**, 064406 (2010).

Supplementary Information for Complex field-induced states in Linarite $PbCuSO_4(OH)_2$ with a variety of high-order exotic SDW_p states

B. Willenberg[1,2], M. Schäpers[3], A.U.B. Wolter[3], S.-L. Drechsler[3], M. Reehuis[2], B. Büchner[3,4], A.J. Studer[5], K.C. Rule[5], B. Ouladdiaf[6], S. Süllow[1], and S. Nishimoto[3,4]

[1] *Institute for Condensed Matter Physics, TU Braunschweig, D-38106 Braunschweig, Germany*
[2] *Helmholtz Center Berlin for Materials and Energy, D-14109 Berlin, Germany*
[3] *Leibniz Institute for Solid State and Materials Research IFW Dresden, D-01171 Dresden, Germany*
[4] *Institut für Festkörperphysik, TU Dresden, D-01062 Dresden, Germany*
[5] *The Bragg Institute, ANSTO, Kirrawee DC NSW 2234, Australia*
[6] *Institute Laue-Langevin, F-38042 Grenoble Cedex, France*

In this Supplementary part we present the magnetic phase diagram of linarite $PbCuSO_4(OH)_2$ with $H \parallel b$ axis for the convenience of the reader once again, but now extended by the inclusion of new NMR data and under consideration of additional neutron scattering data taken in magnetic fields. These new data establish phase V as a distinct thermodynamic phase. Furthermore, the evolution of the ^{1}H-NMR spectra in phase III is shown as a function of the magnetic field. The nature of the different subspectra are discussed and compared to the ^{1}H-NMR spectra in the phases I and IV. Finally, we explain in more detail the mapping procedure of two coupled $J_1 - J_2$, J_{ic}-chains onto an effective single $\tilde{J}_1$-$\tilde{J}_2$ chain but with a magnetization dependent frustration ratio $\alpha_{\rm eff} = \alpha_{\rm eff}\,(\alpha\,[M/M_s])$.

THE MAGNETIC PHASE DIAGRAM OF LINARITE FOR $H \parallel b$

The phase diagram for a magnetic field H applied parallel to the crystallographic b axis of linarite contains five different regions/phases I to V [1–3] (see Fig. S1). The ground state phase I below $\sim 2.5\,$T is formed by an incommensurate (ICM) elliptical helix (ordering wave vector $\boldsymbol{k} = (0\ 0.186\ 0.5)$, moment size $\mu_{ord} \sim 0.64$ to $0.83\,\mu_B$). The field-induced transition from phase I into phase IV involves either a hysteretic transition (region II, below $\sim 0.6\,$K), a direct one (up to $\sim 1.25\,$K), or the transit through a phase III (up to $\sim 1.9\,$K and $3.2\,$T). Region V (up $9.5\,$T) displays only very weak thermodynamic signatures, therefore it was not clear whether it is a distinct thermodynamic phase. This important issue has been settled by ^{1}H-NMR and neutron diffraction measurements presented in this manuscript. The transition temperatures into phase V obtained from the temperature dependence of our ^{1}H-NMR spectra are included in Fig. S1 for the first time.

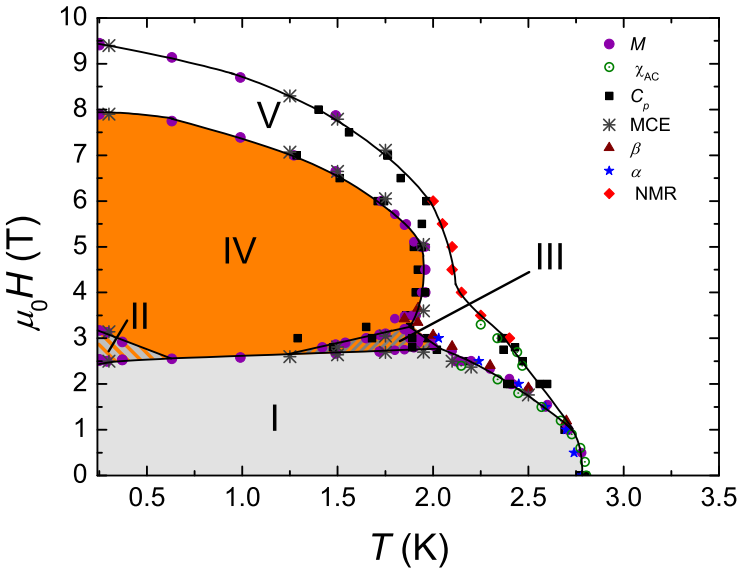

FIG. S1. Phase diagram of linarite with the applied field along the crystallographic b axis. For a brief description of the phases I to V see text and Refs. 1-3. Transition temperatures obtained from new ^{1}H-NMR data are depicted as red diamonds.

NATURE OF THE ^{1}H-NMR SPECTRA IN PHASE III

Phase III is wedged in between phase I and phase IV in the magnetic phase diagram of linarite for $H \parallel b$. From the thermodynamic studies it was speculated that phase III is part of a two-step spin spiral reorientation process by going from phase I via phase III to phase IV. This notion needs to be verified on a microscopic level by means of a combined NMR and neutron scattering study. Here, additional information on the NMR part is presented.

^{1}H-NMR was measured at 1.7 K in 2.5 and 3.0 T and is shown in Fig. S2(a) and (b). For both fields 12 resonance lines are detected, four of them with a high intensity in the middle of the spectra close to the absolute resonance change $\nu - \nu_\mathrm{L} = 0$ MHz, and eight lines situated at the borders of the spectra. The four high-intensity lines in the middle of the spectra closely resemble the shape of the spectra in phase IV, with the latter shown in Fig. S2(c) for an external field of 3.5 T. In turn, by increasing the external magnetic field from 2.5 to 3 T, the whole spectrum shifts to lower frequencies $\nu - \nu_\mathrm{L}$.

Remarkably, the four lines in the middle gain intensity with increasing field, whereas the remaining eight peaks lose intensity. At 2.5 T the four peaks have a relative intensity of 76 %, which is increased to 96 % at 3.0 T, as determined by integrating the subspectra and assuming constant T_2 times in 2.5 and 3 T for the individual peaks.

The eight-peak subspectrum appears to be discrete, which would point towards an underlying commensurate magnetic structure. However, also here the spin-spin correlation time T_2 is very short, which would hamper identification of a horn-shape spectrum expected for an incommensurate spiral structure (cf. the situation for phase I [3]). Our neutron scattering data in phase III provide evidence for a coexistence of the phase IV commensurate magnetic structure with an incommensurate spin spiral. Then, on the supposition of horn-shaped spectra with pairs of lines reaching from one to the other border of the spectrum, viz., from negative to positive $\nu - \nu_\mathrm{L}$, the intensity in between the peaks is easily suppressed due to T_2 being of the order of 10 μs, resulting in the appearance of seemingly discrete peaks.

Under the assumption that the eight remaining peaks are related to the incommensurate helical ground state (due to the same number of resonance lines), a modification of this structure may be expected at the phase boundary I–III. The abrupt change observed in $\nu - \nu_\mathrm{L}$ at the phase boundary from phase I to III makes a change of the spin structure mandatory. Modifications could be a significant change in (either) the spinning plane, the magnetic moment, or the propagation vector. Hence, the NMR data is fully consistent with the conclusion from neutron scattering, i.e., a coexistence in the sample of a spin spiral with phase IV regions.

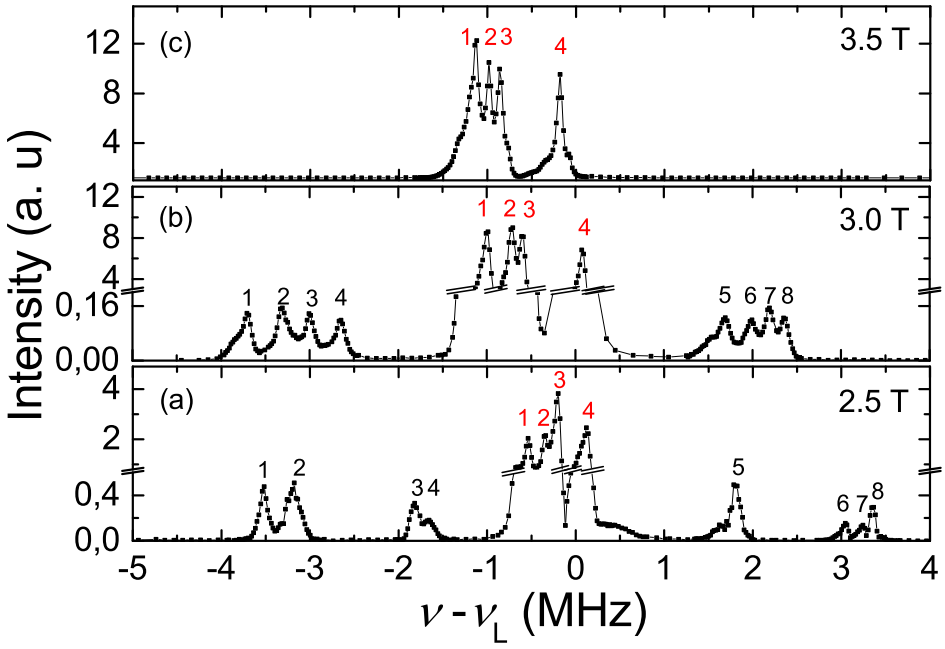

FIG. S2. (a) and (b) ^{1}H-NMR spectra of linarite in phase III at $T = 1.7$ K for $\mu_0 H = 2.5$ and 3.0 T $\parallel b$ axis: Four discrete lines with high intensities (arbitrarily labeled by red numbers) are visible in the middle of each spectrum, which can be associated to the spectra known from phase IV. Eight additional resonance lines (arbitrarily numbered in black) are placed at the border of each spectrum, belonging to a new magnetic structure but which is closely related to the helical magnetic ground state. (c) For comparison, ^{1}H-NMR spectrum of linarite in phase IV at $T = 1.7$ K for $\mu_0 H = 3.5$ T $\parallel b$ axis.

MAPPING OF TWO COUPLED $J_1 - J_2$, J_{ic} CHAINS ONTO AN EFFECTIVE SINGLE $\tilde{J}_1 - \tilde{J}_2$ CHAIN

In the main text, we have performed a mapping from the $J_1 - J_2$ chains weakly coupled by the diagonal interchain exchange interaction J_{ic} (see Fig. S3(a)),

$$\hat{H} = J_1 \sum_{l,i} \mathbf{S}_{l,i} \cdot \mathbf{S}_{l,i+1} + J_2 \sum_{l,i} \mathbf{S}_{l,i} \cdot \mathbf{S}_{l,i+2} + H \sum_{l,i} S^z_{l,i} + J_{ic} \sum_{l,l',i,i'} \mathbf{S}_{l,i} \cdot \mathbf{S}_{l',i'}, \tag{S1}$$

onto an effective single $\tilde{J}_1 - \tilde{J}_2$ chain (see Fig. S3(b)),

$$\hat{H} = \tilde{J}_1 \sum_{i} \mathbf{S}_{i} \cdot \mathbf{S}_{i+1} + \tilde{J}_2 \sum_{i} \mathbf{S}_{i} \cdot \mathbf{S}_{i+2} + H \sum_{i} S^z_{i}, \tag{S2}$$

where $\mathbf{S}_{l,i}$ is a spin-$\frac{1}{2}$ operator at site i in chain l. The objective of this mapping is to mimic the internal magnetic properties of a chain in the coupled $J_1 - J_2$ model by an effective single $\tilde{J}_1 - \tilde{J}_2$ chain. A reliable mapping can be achieved by calculating the dynamical spin structure factor

$$S(\mathbf{q}, \omega) = \sum_{\nu > 0} |\langle \psi_\nu | S(\mathbf{q}) | \psi_0 \rangle| \delta(\omega - (E_\nu - E_0)), \tag{S3}$$

where the static structure factor $S(\mathbf{q})$ is simply the Fourier transform of $S^z_{l,i}$, E_ν and $|\psi_\nu\rangle$ are the ν-th eigenenergy and eigenstate of the system, respectively (the ground state denoted by $\nu = 0$). For some fixed magnetizations M/M_s we determined the value of $\alpha_{eff} = \tilde{J}_2/|\tilde{J}_1|$ to reproduce the spin structure factor of the 15×2 coupled chains by the effective 15-site chain as much as possible. As an example of the mapping, the comparison of the static and dynamical structure factors between the original coupled chains and the effective single chain at $M/M_s = 0.6$ is shown in Fig. S3(c) and (d). We can see a good agreement.

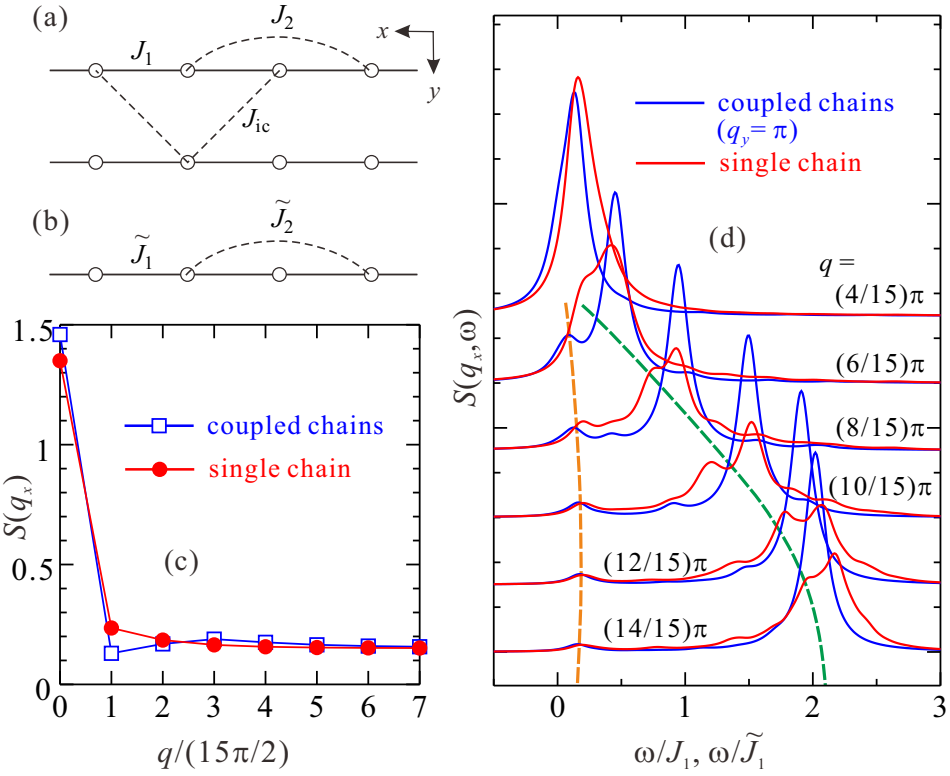

FIG. S3. Lattice models of (a) weakly-coupled $J_1 - J_2$ chains and (b) effective $\tilde{J}_1 - \tilde{J}_2$ chain. (c), (d) Comparison of the static and dynamical spin structure factors between the weakly-coupled $J_1 - J_2$ chains with $\alpha = J_2/|J_1| = 0.36$, $J_{ic}/|J_1| = 0.1$ (blue) and the effective single $\tilde{J}_1 - \tilde{J}_2$ chain with $\alpha_{eff} = \tilde{J}_2/|\tilde{J}_1| = 0.263$ (red) for a fixed magnetization $M/M_s = 0.6$. The static structure factor of the coupled chains $S(q_x)$ has been averaged over $q_y = 0$ and $q_y = \pi$. The orange and green dotted lines denote the lower and upper bounds of the spinon continuum, respectively.

Notice that the obtained "renormalized" $\alpha_{\rm eff}$ depends naturally on both the bare value α and on the type and strength of the interchain coupling. The smaller the former and the larger the skew interchain couplings are, the smaller is the resulting $\alpha_{\rm eff}$. To illustrate this point, we mention that for larger bare α values above 0.7, as relevant for $LiVCuO_4$, one remains in the $p = 2$-region for all magnetic fields in accord with the data of Mourigal *et al.* [4]. In contrast, for Li_2CuO_2 with a smaller bare $\alpha \approx 0.32$ as compared to linarite one reaches already the ferromagnetic phase with $\alpha_{\rm eff} < 0.25$ [5] in accord with the observed alignment of magnetic momenta along the chains and without any anomalous longitudinal collinear SDW_p states. Finally, since the pitch is only weakly affected by the exchange anisotropy, the inclusion of the last "zigzag" into the curve shown in Fig. 4(d) of the main text obtained from an anisotropic generalization of our single chain Hamiltonian is reasonable (see also the next subsection of the present Supplement).

NEMATIC ($p = 2$) STATE NEAR THE SATURATION

According to preliminary (unpublished) measurements for our title compound the material is highly anisotropic (see also Ref. [6]) and a more general spin model might be provided by a Heisenberg chain with xyz-exchange anisotropy for any $\alpha_{\rm eff}$. Then the Hamiltonian is written as

$$H = \sum_{i,\gamma=x,y,z} \tilde{J}_1^{\gamma} S_i^{\gamma} S_{i+1}^{\gamma} + \tilde{J}_2 \sum_i \mathbf{S}_i \cdot \mathbf{S}_{i+2} + H \sum_i S_i^z, \tag{S4}$$

where S_i^{γ} is the γ component of $\mathbf{S}_i$. The xy components of the first term can be divided into an exchange term $\frac{\tilde{J}_1^x + \tilde{J}_1^y}{4}(S_i^+ S_{i+1}^- + h.c.)$ and a double spin-flip term $\frac{\tilde{J}_1^x - \tilde{J}_1^y}{4}(S_i^+ S_{i+1}^+ + h.c.)$. This term has the same form as the order parameter of the nematic state $\langle S_i^- S_{i+1}^- \rangle$. It might be dominant at high magnetization $M/M_{\rm s} \sim 1$. Therefore, qualitatively a nematic state might be expected near the saturation in the presence of an xyz-exchange anisotropy. More details will be published elsewhere.

[1] B. Willenberg, M. Schäpers, K. C. Rule, S. Süllow, M. Reehuis, H. Ryll, B. Klemke, K. Kiefer, W. Schottenhamel, B. Büchner, B. Ouladdiaf, M. Uhlarz, R. Beyer, J. Wosnitza, and A. U. B. Wolter, Phys. Rev. Lett. **108**, 117202 (2012).

[2] M. Schäpers, A. U. B. Wolter, S.-L. Drechsler, S. Nishimoto, K.-H. Müller, M. Abdel-Hafiez, W. Schottenhamel, B. Büchner, J. Richter, B. Ouladdiaf, M. Uhlarz, R. Beyer, Y. Skourski, J. Wosnitza, K. C. Rule, H. Ryll, B. Klemke, K. Kiefer, M. Reehuis, B. Willenberg, and S. Süllow, Phys. Rev. B **88**, 184410 (2013).

[3] M. Schäpers, H. Rosner, S.-L. Drechsler, S. Süllow, R. Vogel, B. Büchner, and A. U. B. Wolter, Phys. Rev. B **90**, 224417 (2014).

[4] M. Mourigal, M. Enderle, B. Fåk, R. K. Kremer, J. M. Law, A. Schneidewind, A. Hiess, and A. Prokofiev, Phys. Rev. Lett. **109**, 027203 (2012).

[5] W. E. A. Lorenz, R. O. Kuzian, S.-L. Drechsler, W.-D. Stein, N. Wizent, G. Behr, J. Málek, U. Nitzsche, H. Rosner, A. Hiess, W. Schmidt, R. Klingeler, M. Loewenhaupt, and B. Büchner, Europhys. Lett. **88**, 37002 (2009).

[6] A. U. B. Wolter, F. Lipps, M. Schäpers, S.-L. Drechsler, S. Nishimoto, R. Vogel, V. Kataev, B. Büchner, H. Rosner, M. Schmitt, M. Uhlarz, Y. Skourski, J. Wosnitza, S. Süllow, and K. C. Rule, Phys. Rev. B **85**, 014407 (2012).